Theoret. Chim. Acta (Berl.) 37, 89—104 (1975)

Commentationes

Molecular Structure, Quadrupole Splitting, and Magnetic Susceptibility of Iron in Deoxygenated Myoglobin and Hemoglobin*

Alfred Trautwein
Fachbereich Angewandte Physik, Universität des Saarlandes, Saarbrücken, W-Germany

Reinhart Zimmermann
Physikalisches Institut II, Universität Erlangen, W-Germany

Frank E. Harris
Department of Physics, University of Utah, Salt Lake City

Received August 12, 1974

For three stereo-structural models of deoxymyoglobin (Mb) and deoxyhemoglobin (Hb) we derive electronic configurations and their mutual spin-orbit coupling. From the temperature dependent molecular electric field gradient (EFG) tensor we calculate temperature dependent quadrupole splittings, $\Delta E_Q(T)$, asymmetry parameters, $\eta(T)$, and orientations of the EFG component $V_{zz}(T)$ with respect to the heme group. Comparing theoretical and experimental data we find a molecular electronic structure, which then is used to compute temperature dependent magnetic susceptibilities, $\chi(T)$. Theoretical and experimental $\chi(T)$ data are in reasonable agreement. From the consistency of our model calculations with experimental results we conclude that iron in Mb and Hb probably is penta-coordinated and considerably out of the heme plane by 0.4–0.8 Å.

Key words: Myoglobin, deoxygenated, quadrupole splitting – Hemoglobin, deoxygenated, quadrupole splitting

1. Introduction

Since the classical work on "Electric Field Gradient Tensors in Ferrous Compounds" by Ingalls [1] several attempts [2–9] have been carried out to calculate temperature dependent contributions to the electric field gradient tensor (V_{pq}) and susceptibility tensor (χ_{pq}) in ferrous compounds in order to fit temperature dependent experimental quadrupole splittings, $\Delta E_Q(T)$, and susceptibilities, $\chi(T)$. All these calculations were based on a crystal field picture which included next nearest neighbour effects in a more or less integral form via crystal field potentials and isotropic covalency factors acting on iron orbitals. The purpose of this contribution is to derive a model for the evaluation of temperature dependent V_{pq} and χ_{pq} contributions including these neighbour effects in a more

* Supported in part by Stiftung Volkswagenwerk, by Deutsche Forschungsgemeinschaft, by the European Molecular Biology Organization, by an award from the Biomedical Sciences Support Grant at the University of Utah, and the National Science Foundation.

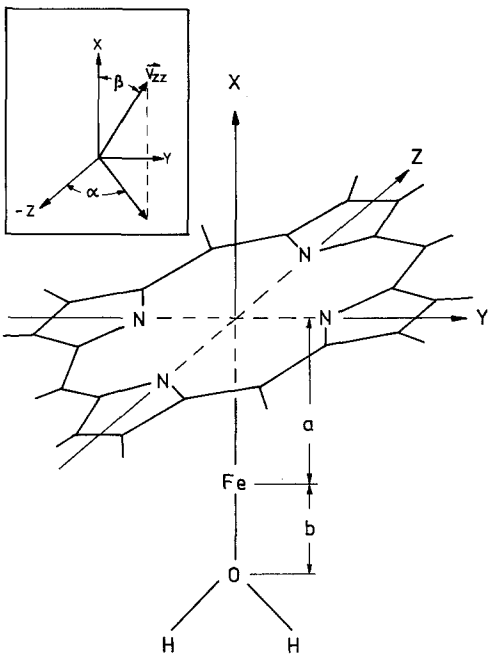

Fig. 1. Stereostructural models for Mb or Hb: (I) $a=0.4$ Å, $b=2.09$ Å; (II) $a=0.4$ Å, $b=2.34$ Å; (III) $a=0.8$ Å, $b=2.34$ Å

direct form. We shall apply this model then to the ferrous high-spin compounds deoxymyoglobin (Mb) and deoxyhemoglobin (Hb) and compare our theoretical results with experiments and findings of other authors.

1.1. Models for Mb *and* Hb

The stereostructural models we use for Mb and Hb are shown in Fig. 1. The three different models in Fig. 1 are denoted by I, II, and III, respectively. The cartesian coordinates of the heme atoms involved in our molecular orbital (MO) calculations are those of Zerner, Gouterman and Kobayashi [10] which are based on Koenig's [11] X-ray data on hemin. The histidine, which binds to the fifth coordination of the heme iron, is simulated in the present work by a water molecule. It is common to all three models that the ferrous iron is pentacoordinated and out of the heme plane. This assumption will be discussed with respect to recent X-ray data on deoxyhemoglobin [12] at the end of Section 6.

2. Quadrupole Splitting and Electric Field Gradient Tensor

From the calculated electronic structures for Models I, II, and III we obtain quadrupole splittings

$$\Delta E_Q = \tfrac{1}{2} e Q V_{zz} (z + \tfrac{1}{3}\eta^2)^{1/2} \tag{1}$$

The nuclear quadrupole moment Q is taken to be $+0.21$ b, consistently with our previous work [13–15] and the finding of other authors [16]. The main component of the EFG tensor, V_{zz}, is defined by $|V_{zz}| \geqq |V_{yy}| \geqq |V_{xx}|$ and results together with the asymmetry parameter

$$\eta = \frac{|V_{xx} - V_{yy}|}{|V_{zz}|} \tag{1a}$$

from diagonalizing the EFG tensor V_{pq}, which contains valence and lattice contributions:

$$V_{pq} = V_{pq}^{\mathrm{val}} + V_{pq}^{\mathrm{lat}};\ p, q = x, y, z\,. \tag{2}$$

The tensor V_{pq}^{val} has been calculated with the equivalence

$$V_{pq}^{\mathrm{val}} = \langle \|\mathrm{EFG}\| \rangle\, e(1-R)\, \langle r^{-3} \rangle\, L_{pq}\,. \tag{2a}$$

The reduced matrix element $\langle \|\mathrm{EFG}\| \rangle$ takes the value $\frac{2}{7}$ for d electrons, $\frac{6}{5}$ for p electrons, and 0 for s electrons. The quantity e represents the (positive!)

Table 1. Matrix elements $\langle \psi_{h'} | l_{pq} | \psi_h \rangle$ with Fe AO's having the sequence $|3d, yz\rangle$, $|3d, xz\rangle$, $|3d, xy\rangle$, $|3d, z^2\rangle$, $|3d, x^2-y^2\rangle$, $|\overline{4s}\rangle$, $|4p, x\rangle$, $|4p, y\rangle$, $|4p, z\rangle$. l_{zz} is obtained from $l_{zz} = -l_{xx} - l_{yy}$

$$l_{xx} = \begin{pmatrix} 2 & 0 & 0 & & & & & & \\ 0 & -1 & 0 & & & & & & \\ 0 & 0 & -1 & & & & & & \\ & & & 1 & \sqrt{3} & & & & \\ & & & \sqrt{3} & -1 & & & & \\ & & & & & 0 & & & \\ & & & & & & -\frac{2}{3} & 0 & 0 \\ & & & & & & 0 & \frac{1}{3} & \\ & & & & & & 0 & 0 & \frac{1}{3} \end{pmatrix} \qquad l_{yy} = \begin{pmatrix} -1 & 0 & 0 & & & & & & \\ 0 & 2 & 0 & & & & & & \\ 0 & 0 & -1 & & & & & & \\ & & & 1 & -\sqrt{3} & & & & \\ & & & -\sqrt{3} & -1 & & & & \\ & & & & & 0 & & & \\ & & & & & & \frac{1}{3} & 0 & 0 \\ & & & & & & 0 & -\frac{2}{3} & 0 \\ & & & & & & 0 & 0 & \frac{1}{3} \end{pmatrix}$$

$$l_{xz} = \tfrac{1}{2} \begin{pmatrix} 0 & 0 & -3 & 0 & 0 & & & & \\ 0 & 0 & 0 & -\sqrt{3} & -3 & & & & \\ -3 & 0 & 0 & & & 0 & & & \\ 0 & -\sqrt{3} & 0 & & & & & & \\ 0 & -3 & 0 & & & & & & \\ & & & & & & 0 & & \\ & & & & & & & 0 & 0 & -1 \\ & & & & & & & 0 & 0 & 0 \\ & & & & & & & -1 & 0 & 0 \end{pmatrix} \qquad l_{yz} = \tfrac{1}{2} \begin{pmatrix} 0 & 0 & 0 & -\sqrt{3} & 3 & & & & \\ 0 & 0 & -3 & 0 & 0 & & & & \\ 0 & -3 & 0 & 0 & 0 & 0 & & & \\ -\sqrt{3} & 0 & 0 & & & & & & \\ 3 & 0 & 0 & & & & & & \\ & & & & & & 0 & & \\ & & & & & & & 0 & 0 & 0 \\ & & & & & & & 0 & 0 & -1 \\ & & & & & & & 0 & -1 & 0 \end{pmatrix}$$

$$l_{xy} = \tfrac{1}{2} \begin{pmatrix} 0 & -3 & 0 & 0 & 0 & & & & \\ -3 & 0 & 0 & 0 & 0 & & & & \\ 0 & 0 & 0 & 2\sqrt{3} & 0 & & & & \\ 0 & 0 & 2\sqrt{3} & & & 0 & & & \\ 0 & 0 & 0 & & & & & & \\ & & & & & & 0 & & \\ & & & & & & & 0 & -1 & 0 \\ & & & & & & & -1 & 0 & 0 \\ & & & & & & & 0 & 0 & 0 \end{pmatrix}$$

elementary charge, and $\langle r^{-3}\rangle$ is the radial factor resulting from taking the expectation value of $(3z^2-r^2)/r^5$. The $\langle r^{-3}\rangle_{3d}$ are taken from estimates [17] based on Clementi's [18] atomic Hartree-Fock wavefunctions: 4.49 a.u. for Fe configuration $3d^7$, 5.09 a.u. for $3d^6$, and 5.73 a.u. for $3d^5$. The actual value of $\langle r^{-3}\rangle_{3d}$ is determined for each model from its calculated Fe $3d$ orbital occupancy by interpolation between the foregoing values. The Sternheimer shielding correction [19] is taken as $(1-R)_{3d}=0.68$. Since we find for the three models under study the configuration $3d^{6.25}$ from MO calculations we derive for

$$\Delta E_Q^0=\tfrac{1}{2}e^2Q(1-R)_{3d}\langle r^{-3}\rangle_{3d}\tfrac{4}{7}$$

the value 4.1 mm/sec. For Fe $4p$ electrons the quantity $(1-R)_{4p}\langle r^{-3}\rangle_{4p}$ is taken to be $\frac{1}{3}$ of the corresponding quantity for the $3d$ electrons [15, 20]. Finally the tensor components L_{pq} result from an appropriate summation over expectation values $\langle\psi_{h'}|\underline{l_{pq}}|\psi_h\rangle$, where $\psi_{h'}$ and ψ_h are single-electron atomic orbitals (AO) of iron, and the single-electron operators $\underline{l_{pq}}$ acting on ψ_h are:

$$\underline{l_{pq}}=\tfrac{1}{2}(\underline{l_p}\,\underline{l_q}+\underline{l_q}\,\underline{l_p})-\tfrac{1}{3}\underline{l}(\underline{l}+1)\,\delta_{pq}\,. \tag{3}$$

For iron $3d$, $4s$, and $4p$ AO's all possible matrix elements $\langle\psi_{h'}|\underline{l_{pq}}|\psi_h\rangle$ are summarized in Table 1.

3. Spin Orbit Coupling and Temperature Dependent EFG Tensor

In high-spin ferrous compounds we are concerned with electronic states $|\Gamma,\gamma,S,\gamma_S\rangle$ characterized by irreducible representations Γ and by total spin $S=2$. All irreducible representations Γ of the regarded symmetry group C_{2v} are one-dimensional and thus γ can be omitted. For convenience the spin states $|S,\gamma_S\rangle$ are linear combinations of the spin states $|S,m_S\rangle$ which transform according to irreducible representations of C_{2v}. This can be achieved similar to the construction of d-orbitals $|xz\rangle, |yz\rangle,\ldots$ from $|L=2,m_L\rangle$. The fivefold spin degeneracy of each state Γ is lifted by spin-orbit interaction:

$$\underline{H_{\text{S.O.}}}=-\lambda\underline{L}\cdot\underline{S}\,, \tag{4}$$

where the coupling constant λ is commonly related to the free ion value, $\lambda_0=103\ \text{cm}^{-1}$, by a reduction factor α^2: $\lambda=\alpha^2\lambda_0$. The eigenvectors $|e_\alpha\rangle$ of this problem, having energies E_α, are certain linear combinations of the base vectors $|\Gamma,S,\gamma_S\rangle$:

$$|e_\alpha\rangle=\sum_{\Gamma,\gamma_S}C^\alpha_{\Gamma,\gamma_S}|\Gamma,S,\gamma_S\rangle\,. \tag{5}$$

The coefficients $C^\alpha_{\Gamma,\gamma_S}$ and the corresponding energies E_α result from diagonalizing the spin-orbit interaction matrix $\langle\Gamma',S,\gamma'_S|\underline{H_{\text{S.O.}}}|\Gamma,S,\gamma_S\rangle$. Since we are interested in quadrupole splittings, ΔE_Q, we calculate for each state $|e_\alpha\rangle$ its relevant EFG tensor:

$$V^\alpha_{pq}=\langle e_\alpha|\,\underline{V_{pq}}|e_\alpha\rangle\,. \tag{6}$$

In order to evaluate the temperature dependence of the EFG one must average the components V_{pq}^{α} of the individual substates $|e_\alpha\rangle$ according to Boltzmann-statistics:

$$\langle V_{pq}\rangle_T = \sum_\alpha V_{pq}^\alpha \exp\left(-\frac{E_\alpha}{kT}\right) \Big/ \sum_\alpha \exp\left(-\frac{E_\alpha}{kT}\right). \tag{7}$$

Diagonalization of $\langle V_{pq}\rangle_T + V_{pq}^{\text{lat}}$ leads to $V_{zz}(T)$, to $\eta(T)$, to the orientation of $V_{zz}(T)$, and finally through Eq. (1) to $\Delta E_Q(T)$.

The spin-orbit interaction matrix elements $\langle \Gamma', S, \gamma_S | \underline{H_{\text{S.O.}}} | \Gamma, S, \gamma_S\rangle$ and the EFG tensor elements $\langle \Gamma', S, \gamma_S | \underline{V_{pq}} | \Gamma, S, \gamma_S\rangle$ may be simplified by

$$\begin{aligned} \langle \Gamma', S, \gamma_S | \lambda \underline{L}\cdot\underline{S} | \Gamma, S, \gamma_S\rangle &= \lambda \langle \Gamma' | \underline{L} | \Gamma\rangle \langle S, \gamma_S' | \underline{S} | S, \gamma_S\rangle , \\ \langle \Gamma', S, \gamma_S' | \underline{V_{pq}} | \Gamma, S, \gamma_S\rangle &= \langle \Gamma' | \underline{V_{pq}} | \Gamma\rangle \delta_{\gamma_S' \gamma_S} . \end{aligned} \tag{8}$$

The evaluation of matrix elements $\langle \Gamma' | Q | \Gamma\rangle$, with $Q = \underline{V_{pq}}$ or $\underline{L_p}$ will be discussed in the following section.

4. Spin-Orbit Interaction Matrix and EFG Tensor Derived from Many-Electron-MO Wave Functions

Iterative extended Hückel calculations are carried out for Models I, II, and III to find linear combinations of atomic orbitals by methods described in detail previously [13, 21], and applied already to CO-myoglobin [22]. From the Hückel one-electron wave functions $\phi_k = \Sigma_h a_{kh}\psi_h$ with ϕ_k representing MO's and ψ_k AO's, we build up configurations (CFG) by constructing appropriate Slater-determinants $|\text{CFG}; \overline{k}_1, \ldots, \overline{k}_m\rangle \equiv \{\phi_{\overline{k}_1}, \ldots, \phi_{\overline{k}_m}\}$.

Here $\phi_{\overline{k}_i}$ is a molecular spin orbital (MSO). If the CFG's describing high-spin ferrous states are different from each other by only a single MSO, which may be denoted by $\overline{k}$ we write $|\text{CFG}, \overline{k}\rangle \equiv \{\phi_{\overline{k}_1}, \ldots, \phi_{\overline{k}_{m-1}}, \phi_{\overline{k}}\}$. Taking into account configuration interaction, CI, we may get new terms $|\text{CI}, l\rangle$ which are in general linear combinations of $|\text{CFG}, \overline{k}\rangle$:

$$|\text{CI}, l\rangle = \sum_{\overline{k}} m_{l\overline{k}} |\text{CFG}, \overline{k}\rangle . \tag{9}$$

With the wavefunctions defined in Eq. (9) we now calculate matrix elements of the operator Q, which for our purpose stands for the orbital angular momentum $\underline{L_p}$ or the EFG tensor operator $\underline{V_{pq}}$. We obtain

$$\langle \text{CI}, l' | Q | \text{CI}, l\rangle = \sum_{\overline{k}', \overline{k}} m_{l'\overline{k}'} m_{l\overline{k}} \langle \text{CFG}, \overline{k}' | Q | \text{CFG}, \overline{k}\rangle . \tag{10}$$

The matrix elements $\langle \text{CFG}, \overline{k}' | Q | \text{CFG}, \overline{k}\rangle$ in Eq. (10) are represented by [23]

$$\langle \text{CFG}, \overline{k}' | Q | \text{CFG}, \overline{k}\rangle = \langle \phi_{\overline{k}} | Q | \phi_{\overline{k}}\rangle + \sum_{i=1}^{m-1} \langle \phi_{k_i} | Q | \phi_{k_i}\rangle \tag{11a}$$

for $\overline{k}' = \overline{k}$, and

$$\langle \text{CFG}, \overline{k}' | Q | \text{CFG}, \overline{k}\rangle = \langle \phi_{\overline{k}'} | Q | \phi_{\overline{k}}\rangle \tag{11b}$$

for $\overline{k}' \neq \overline{k}$.

Using the convention $k=\bar{k}$, k_i the quantities $\langle\phi_{k'}|\,Q|\phi_k\rangle$ are given in terms of AO's by:

$$\langle\phi_{k'}|\,Q|\phi_k\rangle=\sum_{h',h} a_{k'h'}a_{kh}\langle\psi_{h'}|\,Q|\psi_h\rangle\,. \tag{12}$$

Thus Eq. (10) becomes:

$$\langle \mathrm{CI}, l'|\,Q|\mathrm{CI}, l\rangle=\sum_{h',h} C_{(l'l)(h'h)}\langle\psi_{h'}|\,Q|\psi_h\rangle\,, \tag{13}$$

where the coefficients $C_{(l'l)(h'h)}$ are defined by

$$C_{(l'l)(h'h)}=\delta_{l'l}C_{h'h}+\bar{C}_{(l'l)(h'h)}$$

and

$$C_{h'h}=\sum_k a_{kh'}a_{kh}\,,$$

$$\bar{C}_{(l'l)(h'h)}=\sum_{k'} m_{l'k'}a_{k'h'}\sum_k m_{lk}a_{kh}\,.$$

Now, concerning $\langle\psi_{h'}|\,Q|\psi_h\rangle$ of Eq. (13) we distinguish three different matrix elements, $\langle\psi_{h'}|\,Q|\psi_h\rangle$, $\langle\psi_{h'}|\,Q|\psi_{h''}\rangle$, and $\langle\psi_{h''}|\,Q|\psi_{h'''}\rangle$, where the indices h, h' stand for Fe AO's and h'', h''' for ligand AO's, respectively. With this convention we rewrite Eq. (13) into:

$$\begin{aligned}\langle \mathrm{CI}, l'|\,Q|\mathrm{CI}, l\rangle=&\sum_{h',h} C_{(l'l)(h'h)}\langle\psi_{h'}|\,Q|\psi_h\rangle\\&+\sum_{h',h''}\left(C_{(l'l)(h'h'')}\pm C_{(l'l)(h''h')}\right)\langle\psi_{h'}|\,Q|\psi_{h''}\rangle\\&+\sum_{h'',h'''} C_{(l'l)(h''h''')}\langle\psi_{h''}|\,Q|\psi_{h'''}\rangle\,.\end{aligned} \tag{14}$$

The $+$-sign in Eq. (14) corresponds to the case where Q represents a real operator (EFG), the $-$-sign to the case where Q represents a complex operator (orbital momentum). The matrix elements $\langle\psi_{h'}|\,Q|\psi_{h''}\rangle$ representing cross-terms between iron AO's and ligand AO's can be transformed by introducing a completeness relation of orthogonal orbitals $|\psi_{\bar{h}}\rangle$ which contain the iron AO's $|\psi_{h'}\rangle$:

$$\langle\psi_{h'}|\,Q|\psi_{h''}\rangle=\sum_{\bar{h}}\langle\psi_{h'}|\,Q|\psi_{\bar{h}}\rangle\langle\psi_{\bar{h}}|\psi_{h''}\rangle\,. \tag{15}$$

If Q does not lead out of the subspace of $|\psi_{h'}\rangle$, the summation can be restricted to iron orbitals, and we obtain:

$$\langle\psi_{h'}|\,Q|\psi_{h''}\rangle=\sum_h\langle\psi_{h'}|\,Q|\psi_h\rangle\,S_{hh''}\,, \tag{16}$$

where $S_{hh''}$ stands for the overlap integrals between iron AO's ψ_h and ligand AO's $\psi_{h''}$ (cf. "Note Added in Proof").

With the use of Eqs. (14) and (16) we are able to calculate matrix elements for the spin-orbit interaction and for the EFG tensor. For the evaluation of matrix elements $\langle|\underline{H_{\mathrm{S.O.}}}|\rangle$ from Eq. (14) we use the $-$-sign and neglect the pure ligand contributions $\langle\psi_{h''}|\,\underline{H_{\mathrm{S.O.}}}|\psi_{h'''}\rangle$.

In the case of the EFG we derive V_{pq} by using the $+$-sign in Eq. (14), and we distinguish two parts, 1. the so-called valence contribution

$$\langle l'|\,\underline{V_{pq}^{\mathrm{val}}}|l\rangle=\sum_{h',h}\left[C_{(l'l)(h'h)}+\sum_{h''}\left(C_{(l'l)(h'h'')}+C_{(l'l)(h''h')}\right)S_{hh''}\right]\langle\psi_{h'}|\,\underline{V_{pq}}|\psi_h\rangle\,, \tag{17}$$

with $\langle \psi_{h'} | \underline{V_{pq}^{\mathrm{val}}} | \psi_h \rangle$ being obtained from Eqs. (2a) and (3), and 2. the so-called lattice contribution

$$\langle l' | \underline{V_{pq}^{\mathrm{lat}}} | l \rangle = \sum_{h'',h'''} C_{(l'l)(h''h''')} \langle \psi_{h''} | \underline{V_{pq}} | \psi_{h'''} \rangle . \tag{18}$$

Assuming the ligand charges q_a to be localized at lattice points (R_{xa}, R_{ya}, R_{za}) we can approximate V_{pq}^{lat} of Eq. (18) by

$$\langle l' | \underline{V_{pq}^{\mathrm{lat}}} | l \rangle = (1-\gamma_\infty) \sum_a q_a (3R_{pa}R_{qa} - \delta_{pq}R_a^2)/R_a^5 , \tag{19}$$

where q_a and (R_{xa}, R_{ya}, R_{za}) are the charge and the cartesian coordinates of the a^{th} ligand, and $(1-\gamma_\infty)$ represents the Sternheimer antishielding [19] of iron core electrons due to ligand charges.

From our MO calculations we get the information concerning the coefficients $C_{(l'l)(h'h)}$ and $C_{(l'l)(h'h'')}$, the overlaps $S_{hh''}$, and the atomic charges q_a. Thus the problem of calculating $\Delta E_Q(T)$, $\eta(T)$, and the orientation of the EFG component V_{zz} is solved straightforward using the formalism described in the foregoing sections, and identifying states $|\mathrm{CI}, l\rangle$ and $|\Gamma, S, \gamma_S\rangle$ through the transformation properties of $|\mathrm{CI}, l\rangle$.

5. Results

Carrying out calculations for the Models I, II, and III we make approximations which have to be discussed before presenting the computational results. We restrict spin-orbit interaction to states which we find to be lowest in energy by configuration interaction (CI) calculations[1]. According to C_{2v} symmetry of the three models presently under study these states (see Fig. 2) are characterized by irreducible representations $^5A_2$, $^5B_1$, and $^5B_2$ [24]. To study the effect of an energetically low lying low-spin term on $\Delta E_Q(T)$ and $\eta(T)$ we add the state $^1A_1$ (Fig. 2) to our investigation. Since the four states have different irreducible representations the coefficient matrix $m_{l\tilde{k}}$ of Eq. (9) will remain diagonal independent of the energy separations of the four states. Thus we get the simple relation

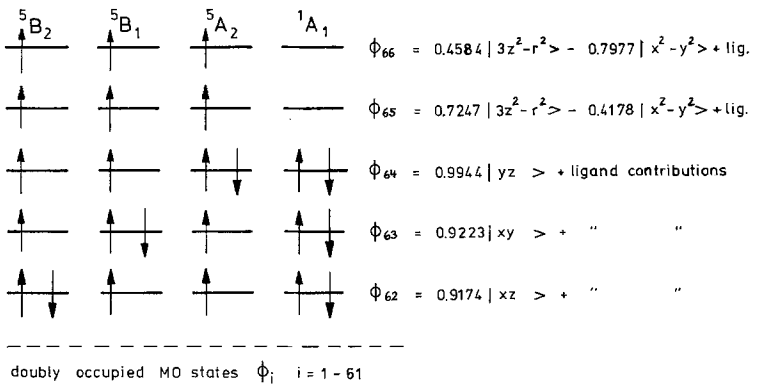

Fig. 2. Many-electron states which are used to calculate $\Delta E_Q(T)$, $\eta(T)$, and $\chi(T)$. The coefficients of ϕ_{i+n} represent the situation for Model (I) of Fig. 1

[1] The configuration interaction procedure is described in Ref. [13].

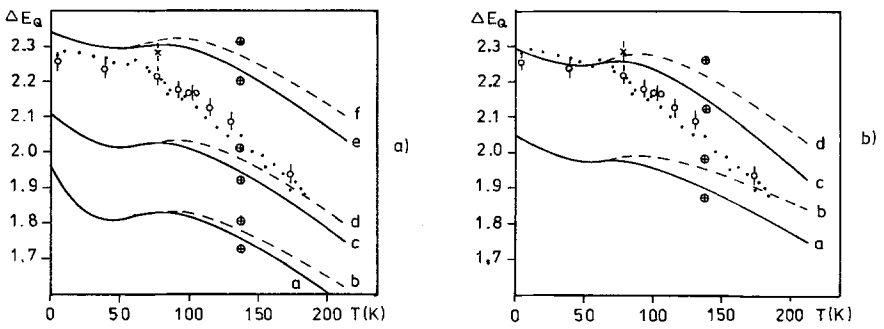

Fig. 3a and b. Temperature dependent quadrupole splittings for Model (III). $\lambda = 90\ \mathrm{cm}^{-1}$. Experimental $\Delta E_Q(T)$ data for frozen Mb solution (Ref. [26]) are indicated by closed circles, for a Mb single crystal (Ref. [27]) by "X" and error bars, and for frozen Hb (rat) solution (Refs. [2, 3]) by open circles and error bars. Energies for $^5B_2$, $^5B_1$, $^5A_2$, and $^1A_1$ in cm^{-1} corresponding to $\Delta E_Q(T)$ curves are:

a	*a*	0,	150,	100,	50
	b	0,	150,	100,	10000
	c	0,	200,	100,	50
	d	0,	200,	100,	10000
	e	0,	300,	100,	50
	f	0,	300,	100,	10000
b	*a*	0,	50,	300,	50
	b	0,	50,	300,	10000
	c	0,	100,	300,	50
	d	0,	100,	300,	10000

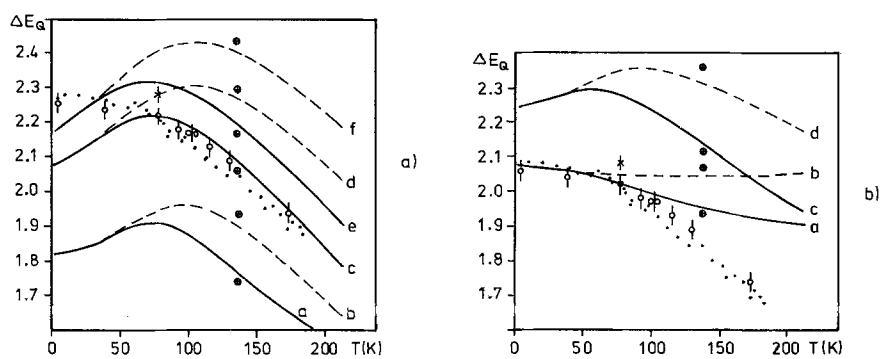

Fig. 4a and b. Temperature dependent quadrupole splittings for Model (III). $\lambda = 90\ \mathrm{cm}^{-1}$. Experimental $\Delta E_Q(T)$ data are defined in Fig. 3. Energies for $^5B_2$, $^5B_1$, $^5A_2$, and $^2A_1$ in cm^{-1} corresponding to $\Delta E_Q(T)$ curves are:

a	*a*	300,	0,	300,	50
	b	300,	0,	300,	10000
	c	600,	0,	300,	50
	d	600,	0,	300,	10000
	e	1000,	0,	300,	50
	f	1000,	0,	300,	10000
b	*a*	50,	0,	800,	50
	b	50,	0,	800,	10000
	c	200,	0,	800,	50
	d	200,	0,	800,	10000

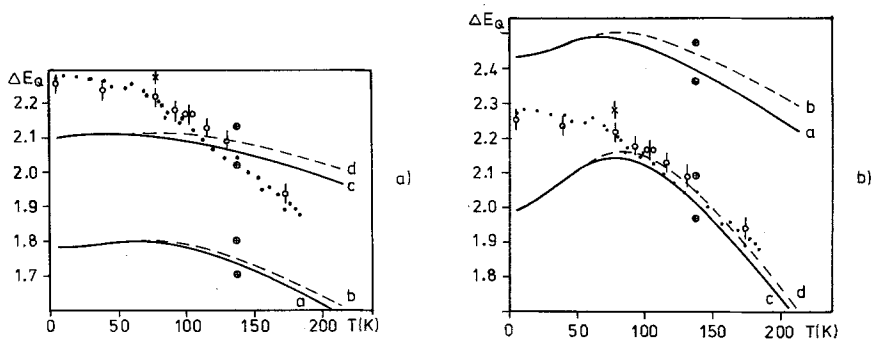

Fig. 5a and b. Temperature dependent quadrupole splittings for Model (III). $\lambda = 90\ \mathrm{cm}^{-1}$. Experimental $\Delta E_Q(T)$ data are defined in Fig. 3. Energies for $^5B_2$, $^5B_1$, $^5A_2$, and $^1A_1$ in cm^{-1} corresponding to $\Delta E_Q(T)$ curves are:

a	*a*	100,	300,	0,	50
	b	100,	300,	0,	10000
	c	100,	500,	0,	50
	d	100,	500,	0,	10000
b	*a*	200,	800,	0,	50
	b	200,	800,	0,	10000
	c	300,	300,	0,	50
	d	300,	300,	0,	10000

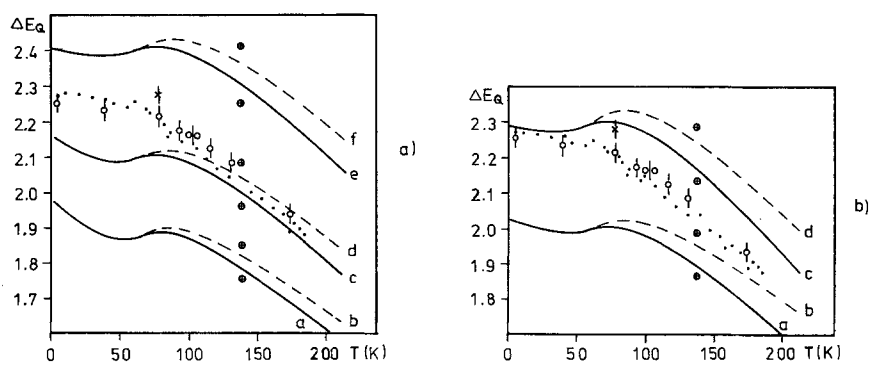

Fig. 6a and b. Temperature dependent quadrupole splittings for Model (I). $\lambda = 90\ \mathrm{cm}^{-1}$. Experimental $\Delta E_Q(T)$ data are defined in Fig. 3. Energies for $^5B_2$, $^5B_1$, $^5A_2$, and $^1A_1$ in cm^{-1} corresponding to $\Delta E_Q(T)$ curves are:

a	*a*	0,	150,	150,	50
	b	0,	150,	150,	10000
	c	0,	200,	150,	50
	d	0,	200,	150,	10000
	e	0,	300,	150,	50
	f	0,	300,	150,	10000
b	*a*	0,	100,	300,	50
	b	0,	100,	300,	10000
	c	0,	150,	300,	50
	d	0,	150,	300,	10000

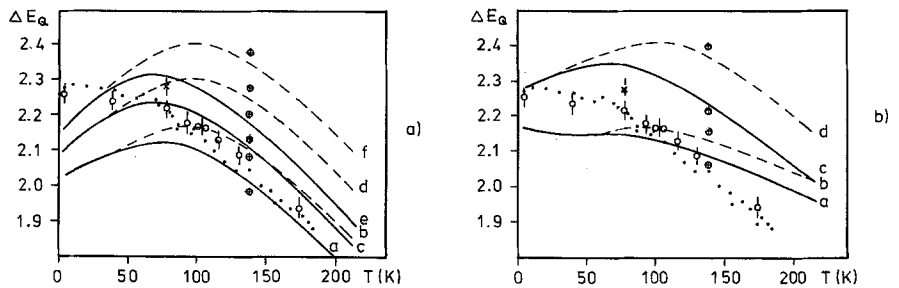

Fig. 7a and b. Temperature dependent quadrupole splittings for Model (II). $\lambda = 90\,\mathrm{cm}^{-1}$. Experimental $\Delta E_Q(T)$ data are defined in Fig. 3. Energies for $^5B_2$, $^5B_1$, $^5A_2$, and $^1A_1$ in cm^{-1} corresponding to $\Delta E_Q(T)$ curves are:

a	*a*	0,	300,	400,	50
	b	0,	300,	400,	10000
	c	0,	300,	600,	50
	d	0,	300,	600,	10000
	e	0,	300,	1000,	50
	f	0,	300,	1000,	10000
b	*a*	0,	400,	200,	50
	b	0,	400,	200,	10000
	c	0,	400,	400,	50
	d	0,	400,	400,	10000

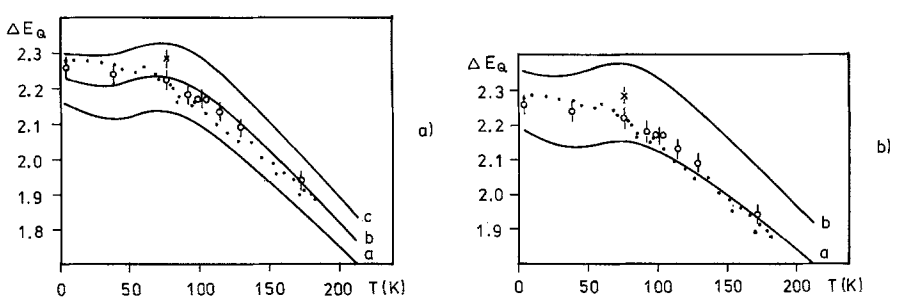

Fig. 8a and b. Temperature dependent quadrupole splittings for Model (I). $\lambda = 75\,\mathrm{cm}^{-1}$. Experimental $\Delta E_Q(T)$ data are defined in Fig. 3. Energies for $^5B_2$, $^5B_1$, $^5A_2$, and $^1A_1$ in cm^{-1} corresponding to $\Delta E_Q(T)$ curves are:

a	*a*	0,	150,	150,	10000
	b	0,	150,	175,	10000
	c	0,	150,	200,	10000
b	*a*	0,	200,	100,	10000
	b	0,	200,	150,	10000

$|\mathrm{CI}, l\rangle = |\mathrm{CFG}, \overline{k}\rangle$ instead of Eq. (9). This allows us to vary the mutual energy separations between $^5A_2$, $^5B_1$, $^5B_2$, and $^1A_1$ without changing the states $|\mathrm{CI}, l\rangle$.

For each of the three models we then carry out calculations along the lines described above to get $\Delta E_Q(T)$, $\eta(T)$, sign V_{zz}, and the orientation of V_{zz} relative to the heme-coordinate system of Fig. 1. Some of the resulting $\Delta E_Q(T)$-curves for various energies $E(^5A_2)$, $E(^5B_1)$, $E(^5B_2)$, and $E(1A_1)$ are shown in Figs. 3–7 for

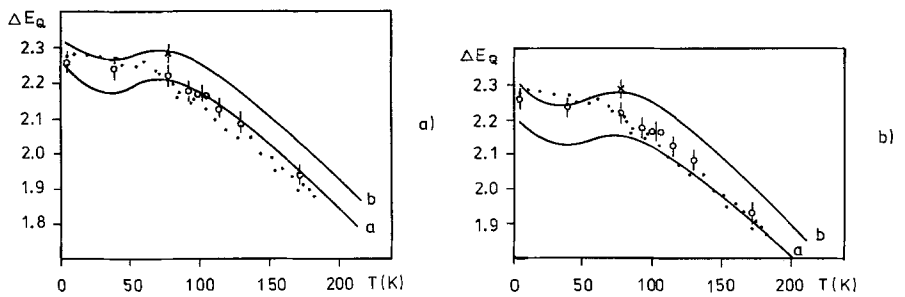

Fig. 9a and b. Temperature dependent quadrupole splittings for Model (III). $\lambda = 75\ \mathrm{cm}^{-1}$. Experimental $\Delta E_Q(T)$ data are defined in Fig. 3. Energies for $^5B_2$, $^5B_1$, $^5A_2$, and $^1A_1$ in cm^{-1} corresponding to $\Delta E_Q(T)$ curves are:

a	*a*	0,	120,	160,	10000
	b	0,	120,	180,	10000
b	*a*	0,	180,	100,	10000
	b	0,	180,	120,	10000

Table 2. Energies of spin quintet states (in cm^{-1}), temperature dependent quadrupole splittings (in mm/sec), and asymmetry parameters. The angles α and β (in degrees) defining the orientation of V_{zz} with respect to the heme coordinate system of Fig. 1 are for all Curves 8a and 9a and for temperatures $4.2 \leqq T \leqq 200$ given by $\alpha = 90$, $\beta = 90$

Figure	Curve	Energies of $^5B_2$	$^5B_1$	$^5A_2$	Calculated parameters for temperatures T (in K)	4.2	50	75	100	150	200
8a	*a*	0	150	150	ΔE_Q	2.157	2.118	2.139	2.101	1.934	1.748
					η	0.461	0.436	0.420	0.419	0.447	0.494
	b	0	150	175	ΔE_Q	2.228	2.211	2.235	2.196	2.019	1.820
					η	0.355	0.341	0.327	0.325	0.341	0.377
	c	0	150	200	ΔE_Q	2.299	2.303	2.330	2.290	2.103	1.891
					η	0.249	0.246	0.236	0.230	0.235	0.261
9a	*a*	0	120	160	ΔE_Q	2.242	2.181	2.204	2.175	2.025	1.850
					η	0.369	0.326	0.309	0.307	0.320	0.336
	b	0	120	180	ΔE_Q	2.313	2.269	2.294	2.265	2.112	1.931
					η	0.421	0.371	0.352	0.352	0.372	0.394

spin-orbit coupling constant $\lambda = 90\ \mathrm{cm}^{-1}$, and in Figs. 8 and 9 for $\lambda = 75\ \mathrm{cm}^{-1}$. The + - or − -sign at each curve indicates the calculated sign of the EFG component V_{zz}. The energies, asymmetry parameters, and orientations of V_{zz} corresponding to $\Delta E_Q(T)$-curves of Figs. 8a and 9a are tabulated in Table 2. Experimental $\Delta E_Q(T)$ data for frozen Mb solution [25] are indicated by closed circles, for a Mb single crystal [26] by "x" and error bars, and for frozen Hb (rat) solution [2, 3] by open circles and error bars; the sign of V_{zz} was experimentally determined to be positive from Mb single crystal Mössbauer measurements [26].

6. Discussion

Comparing our theoretical $\Delta E_Q(T)$ curves with the experimental $\Delta E_Q(T)$ data from Mb and Hb we find reasonable coincidence of computational and experimental results only for the case with $^5B_2$ being groundstate (Fig. 8a). From configuration interaction calculations for Model II taking into account configurations $^5B_2$, $^5B_1$, and $^5A_2$ we find $^5B_2$ to be groundstate too. From inspection of Table 2 it is obvious that the $\Delta E_Q(T)$ curve which fits the experimental $\Delta E_Q(T)$ data corresponds to an EFG component V_{zz} being oriented along the heme axis y. This result agrees well with our recent findings from Mössbauer investigation of Mb single crystals at 77 K [26]. There we found an angle of $\alpha = 40° \pm 8°$ between V_{zz} and the crystallographic b-axis of the Mb single crystal, indicating that V_{zz} possibly is oriented along one of the two heme axes y or z.

The asymmetry parameters $\eta(T)$ (from Table 2) which are related with the $\Delta E_Q(T)$ fit Curve b of Fig. 8a also agree with our Mb single crystal Mössbauer results. In Ref. [27] the angle $\alpha = 40° \pm 8°$ was derived assuming η to be zero. A most recent computational analysis of our former Mb single crystal Mössbauer data by Maeda *et al.* (to be published), however, indicate that $\alpha = 40° \pm 8°$ is consistent also with an η-parameter in the range $0 \leqq \eta \leqq 0.3$.

The energy separation $E(^1A_1) - E(^5B_2)$ which is varied between 50 and 10000 cm^{-1} is sensitive only to the slope of the theoretical $\Delta E_Q(T)$ curves for temperatures $T > 50$ K; and, further, $\Delta E_Q(T)$ curves up to $T = 200$ K are identical for $E(^1A_1) - E(^5B_2) = 300\ cm^{-1}$ and $E(^1A_1) - E(^5B_2) = 10000\ cm^{-1}$. Though we find $\Delta E_Q(T)$ curves corresponding to $E(^1A_1) - E(^5B_2) \approx 100\ cm^{-1}$ which fit the experimental $\Delta E_Q(T)$ data we give arguments why an energy separation of $E(^1A_1)\, E(^5B_2) \gtrsim 300\ cm^{-1}$ seems to be more realistic. In addition to the static molecular structure of Fig. 1 we have to consider lattice vibrations which have the effect that the potential V at the iron contains higher terms than the static ligand field potential $V^{(0)}$ [27]:

$$V = V^{(0)} + V^{(1)}\varepsilon + V^{(2)}\varepsilon^2 + \cdots . \tag{20}$$

The quantity ε in Eq. (20) represents an isotropic average of the strain tensor, and $V^{(1)}$, $V^{(2)}$,... describe orbital-lattice interactions. The transition probability of a direct process between states $|a\rangle$ and $|b\rangle$, given by

$$\begin{aligned} W_{ab}^{\mathrm{dir}} &= \frac{2\pi}{\hbar} |\langle a, N-1|\, V^{(1)}\varepsilon |b, N\rangle|^2\, \varrho(E) \\ &= \frac{2\pi}{\hbar} |\langle a|\, V^{(1)}|b\rangle|^2\, |\langle N-1|\, \varepsilon |N\rangle|^2\, \varrho(E)\,, \end{aligned} \tag{21}$$

with $N =$ occupation number of phonons and $\varrho(E) =$ phonon density of final states, is zero if $|a\rangle$ stands for a spin quintet and $|b\rangle$ for a spin singlet, because $V^{(1)}$ is spin-independent and spin-orbit coupling mixes high-spin and low-spin states via spin-triplets only, thus $\langle a|\, V^{(1)}|b\rangle = 0$. In the real case the transition probability W_{ab} might be slightly different from zero since the state $|a\rangle$ ($|b\rangle$) might be a linear combination of a spin quintet (spin singlet) state and a small contribution of its counterpart due to spin-spin interaction. W_{ab} being very small, however, means that the spin-lattice relaxation between $|a\rangle$ and $|b\rangle$ is very slow. With the spin-

lattice relaxation time becoming larger than the precession time of the Fe^{57} nucleus (of order 10^{-7} sec) during γ-absorption and re-emission one would see two separated Mössbauer spectra, one corresponding to the spin quintet $|a\rangle$ and one to the spin singlet $|b\rangle$, and the thermal average for evaluating $\Delta E_Q(T)$ should be only over the high-spin states. There exist several examples for such high-spin low-spin transition in the literature [28] for compounds containing ferrous iron. Believing in slow spin-lattice relaxation between high-spin and low-spin states in deoxygenated myoglobin and hemoglobin one might have the idea to explain Mössbauer spectra of deoxygenated hemoglobins, containing small-intensity lines (see Fig. 4 of Ref. [29]) by thermal mixtures of high-spin and low-spin quadrupole splittings. The ΔE_Q value associated with the $^1A_1$ state of about 1.3 mm/sec would be just in agreement with the "impurity" line positions, however, the intensity ratio, R, of low-spin to high-spin lines would be temperature dependent, in contrast to the experimental results for example of deoxygenated hemoglobin single chains [30], which sometimes, under certain preparational conditions, also show these "impurity" lines. Assuming the $^1A_1$ state to ly in energy above the spin quintet groundstate by 50 cm^{-1} (300 cm^{-1}) the intensity ratio R would be unmeasurably small at $T=4.2$ K; at an elevated temperature of $T=200$ K the ratio R is estimated from energies E_α to be about 8% (2%). For these reasons we believe the energy separation $E(^1A_1)-E(^5B_2)$ to be at least 300 cm^{-1}; thus the spin singlet $^1A_1$ does not influence at all our $\Delta E_Q(T)$-curves.

It remains to compare our present results with ligand field interpretations of temperature dependent quadrupole splittings and susceptibilities of deoxygenated heme compounds by Eicher and Trautwein [2, 3] and by Groves *et al.* [6], and with susceptibility investigations of Mb powder samples[2] by Nakano *et al.* [31]. The ligand field calculations by Eicher and Trautwein [2, 3] were based due to symmetry considerations of the heme group on the assumption that V_{zz} is oriented perpendicular to the heme plane; thus the $^5A_2$ term[2] (using a coordinate system as defined by Fig. 1) was taken as ground state. This situation, however, was ruled out by the present calculations and by our former Mb single crystal experiments [26]. Most recent ligand field calculations by Groves *et al.* [6], basing on the theory described by Eicher *et al.* [2, 3] and taking V_{zz} to be oriented in the heme plane, show that experimental $\Delta E_Q(77\text{ K} \leqq T \leqq 200\text{ K})$ and $\chi(T)$ data are consistent with energy separations of Fe 3d terms of $E(d_{xy})-E(d_{xz})=46$ cm^{-1}, $E(d_{yz})-E(d_{xz})=692$ cm^{-1}, and $E(^1A_1)-E(d_{xz})=333$ cm^{-1}. In these calculations isotropic covalency factors and fast spin-lattice relaxation between high-spin and low-spin states have been assumed, in contrast to our present arguments; further, the $\Delta E_Q(T)$-fit was limited to the temperature range 77 K $\leqq T \leqq$ 200 K only. Keeping in mind that due to these restrictions the energy sequence of states $^5B_1$, $^5B_2$, $^5A_2$, and $^1A_1$, as determined by Groves *et al.* [6], have to be different from ours at least slightly, we notice that their [6] and our present results are mainly consistent: (I) V_{zz} is oriented parallel to the heme plane, (II) $V_{zz}>0$, (III) $\eta \approx 0.5$, (IV) the spin quintet $^5B_2$ is ground state in Mb and Hb, (V) $E(^1A_1)-E(^5B_2) \gtrsim 300$ cm^{-1}, (VI) $E(^5B_1)-E(^5B_2) \lesssim 150$ cm^{-1}, and (VII) $E(^3E_y)-E(^5B_2)>1000$ cm^{-1}.

[2] In the investigation in Refs. [2] and [3] the symmetry was assumed to be C_{4v}. The $^5B_2$ term there corresponds to the irreducible representation $^5A_2$ of the symmetry group C_{2v} in our case (Fig. 1).

To assess further the reliability of our results, which were obtained by fitting experimental quadrupole splittings, we use the energy terms E_α corresponding to Curve b in Fig. 8a and compute temperature dependent magnetic susceptibilities $\chi(T)$. The χ-tensor χ_{pq}, with $p, q = x, y, z$, is defined by

$$\chi_{pq} = \left.\frac{\partial M_p}{\partial H_q}\right|_{H_q \approx 0} \tag{22}$$

M_p represents the magnetization per mole. According to Eq. (22) we may write

$$M_p = \sum_q \chi_{pq} H_q \; ; \tag{22a}$$

and the tensor elements χ_{pq} we derive from

$$\chi_{pq} = \mu_B^2 A \sum_{\alpha,\alpha'} \langle e_\alpha | \underline{L_p} + 2\underline{S_p} | e_{\alpha'} \rangle \langle e_{\alpha'} | \underline{L_q} + 2\underline{S_q} | e_\alpha \rangle \cdot \left[\frac{\exp(-E_{\alpha'}/kT) - \exp(-E_\alpha/kT)}{E_{\alpha'} - E_\alpha} \right]. \tag{23}$$

The spin states $|e_\alpha\rangle$ already have been defined by Eq. (5); and the E_α are their corresponding energies. Symbol A stands for the Avogadro number. For cases of degeneracy we simply take

$$\lim_{E'_\alpha \to E_\alpha} \frac{\exp(-E_{\alpha'}/kT) - \exp(-E_\alpha/kT)}{E_{\alpha'} - E_\alpha} = \frac{\exp(-E_\alpha/kT)}{kT} .$$

The powder susceptibility $\chi(T)$ results from $\chi(T) = \frac{1}{3}\Sigma_p \chi_{pp}$, with $p = x, y, z$. The solid $\chi(T)$ curve in Fig. 10 corresponds to the $\Delta E_Q(T)$ fit Curve *b* in Fig. 8a. Closed circles in Fig. 10 are experimental points taken from the susceptibility investigation of Mb by Nakano *et al.* [32]. The $\chi(T)$ curves corresponding to $\Delta E_Q(T)$ Curve *c* in Fig. 8a and to $\Delta E_Q(T)$ Curves *a* and *b* in Fig. 9a are nearly identical to the solid line of Fig. 10; the broken line, however, represents the situation that spin triplet states ly close to the spin quintet ground state with energy separations $E(^3E_\eta) - E(^5B_2) = 200\ \mathrm{cm}^{-1}$ and $E(^3E_\xi) - E(^5B_2) = 300\ \mathrm{cm}^{-1}$. Thus, by comparing solid line, broken line and experimental points in Fig. 10, we

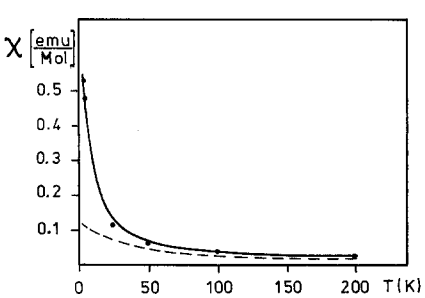

Fig. 10. Temperature dependent susceptibilities. Solid line corresponds to energies as specified for $\Delta E_Q(T)$ Curve *b* of Fig. 8a. Broken line corresponds to energetically low lying spin triplet states (see text). Experimental points are taken from [32]

conclude that the energy sequence $^5B_2$, $^5B_1$, $^5A_2$ give a more realistic picture for deoxygenated heme compounds than the formerly derived ligand field result [2, 3] with an energy sequence of $^5A_2$, ^3E.

Summarizing our results we note that the present MO interpretation of experimental Mössbauer and susceptibility data of deoxygenated heme proteins is approximative in the sense that in the three models under study (Fig. 1) we neglect the protein part of the molecule, several peripheral side chains and the probable non-planarity of the heme group, that we represent the histidine group by a water molecule, and further, that we assume all interatomic distances to remain constant within the whole temperature range of $4.2\,\mathrm{K} \leqq T \leqq 200\,\mathrm{K}$; moreover, the MO-procedure itself is approximative to the extend described in Refs. [13] and [21]. These simplifications, however, are believed to be secondary for the present attempt to derive a gross description of the structural situation of the heme iron in deoxygenated heme compounds. From the present work we therefore conclude that the MO interpretation of experimental Mössbauer and susceptibility data consistently agree with the assumption that the heme iron in Mb and Hb is pentacoordinated and significantly out of "plane" (by $\gtrsim 0.4$ Å; see Fig. 1). The interpretation of recent X-ray data of Mb [32] and of Hb [12] support at least part of our findings, namely that the heme iron in Mb, Hb is pentacoordinated.

References

1. Ingalls, R.: Phys. Rev. **133**, A 787 (1964)
2. Eicher, H., Trautwein, A.: J. Chem. Phys. **50**, 2540 (1969)
   Spiering, H., Zimmermann, R., Ritter, G.: Phys. Stat. Sol. (b) **62**, 123 (1974)
3. Eicher, H., Trautwein, A.: J. Chem. Phys. **52**, 932 (1970)
4. Trautwein, A., Eicher, H., Mayer, A.: J. Chem. Phys. **52**, 2473 (1970)
5. Trautwein, A., Eicher, H., Mayer, A., Alfsen, A., Waks, M., Beuzard, Y., Rosa, J.: J. Chem. Phys. **53**, 963 (1970)
6. Groves, J.: To be published
7. Ok, H. N.: Phys. Rev. B **4**, 3870 (1971)
8. Ganiel, U., Shtrikman, S.: Phys. Rev. **177**, 503 (1969)
9. Perkins, H. K., Hazony, Y.: Phys. Rev. B **5**, 7 (1972)
10. Zerner, H., Gouterman, M., Kobayashi, H.: Theoret. Chim. Acta (Berl.) **6**, 363 (1966)
11. Koenig, D. F.: Acta Cryst. **18**, 663 (1965)
12. Muirhead, H., Greer, J.: Nature **228**, 516 (1970)
13. Trautwein, A., Harris, F. E.: Theoret. Chim. Acta (Berl.) **30**, 45 (1973)
14. Trautwein, A., Kreber, E., Gonser, U., Harris, F. E.: J. Phys. Chem. Sol. (in press)
15. Trautwein, A., Harris, F. E.: Phys. Rev. B **7**, 4755 (1973)
16. Sharma, R. R.: Phys. Rev. Letters **26**, 563 (1971)
17. Weissbluth, M., Maling, J. E.: J. Chem. Phys. **47**, 4166 (1967)
18. Clementi, E.: I.B.M. J. Res. Develop. Suppl. **9**, 2 (1965)
19. Sternheimer, R. M.: Phys. Rev. **130**, 1423 (1963)
20. de Vries, J. L. K. F., Kreijzers, C. P., de Boer, F.: Inorg. Chem. **11**, 1343 (1972)
21. Rein, R., Clarke, G. A., Harris, F. E.: Quantum aspects of heterocyclic compounds in chemistry and biochemistry. The Jerusalem Symposia on Quantum Chemistry and Biochemistry, II. Israel Academy of Sciences and Humanities, Jerusalem 1970
22. Trautwein, A., Maeda, Y., Harris, F. E., Formanek, H.: Theoret. Chim. Acta (Berl.) (in press)
23. Griffith, J. S.: The theory of transition metal ions. Cambridge: University Press 1964
24. Atkins, P. W., Child, M. S., Phillips, C. S. G.: Tables for group theory. Oxford: Oxford University Press 1970

25. Eicher, H., Parak, F., Bade, D., Tejada, X., Kalvius, G. M.: In: Proceedings of the application of the Mössbauer Effect. Bendor, France, Sept. 2–6, 1974
26. Trautwein, A., Maeda, Y., Gonser, U., Parak, F., Formanek, H.: Proceedings of the 5 th international conference in Mössbauer spectroscopy. Bratislava, CSSR, Sept. 1973
Gonser, U., Maeda, Y., Trautwein, A., Parak, F., Formanek, H.: Z. Naturforsch. (in press)
27. Orbach, R.: Proc. Roy. Soc. (London) A **264**, 458 (1961)
28. König, E., Ritter, G.: In: Gruverman (Ed.): Mössbauer effect methodology, Vol. 9. 1974
König, E., Ritter, G., Zimmermann, R.: J. Chem. Phys. (in press)
29. Lang, G., Marshall, W.: Proc. Phys. Soc. **87**, 3 (1966)
30. Alpert, Y., Maeda, Y., Trautwein, A.: Unpublished results
31. Nakano, N., Otsuka, J., Tasaki, A.: Biochim. Biophys. Acta **236**, 222 (1971)
32. Nobbs, C. L., Watson, H. C., Kendrew, J. C.: Nature **209**, 339 (1966)

Prof. Dr. A. Trautwein
Fachbereich 12-1
Angewandte Physik
Universität des Saarlandes
D-6600 Saarbrücken 11
Federal Republic of Germany

Note Added in Proof:

Equation (16) can be applied for $Q = l_p$. If Q is the operator for the EFG, Eq. (16) is only approximatively valid, since the contributions from nondiagonal elements in l (for example contributions $\langle 3d|(\underline{V_{pq}})|4s\rangle$) have been neglected.